

## Resolving Apparent Conflicts between Theoretical and Experimental Models of Phosphate Monoester Hydrolysis

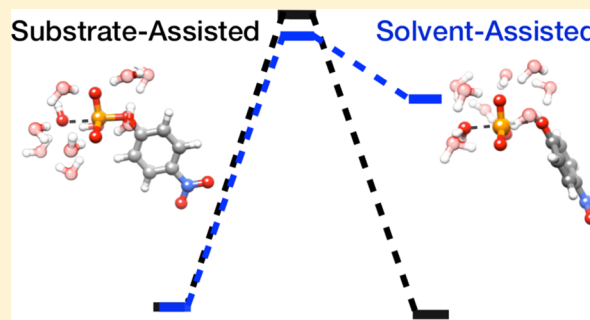
Fernanda Duarte,<sup>†</sup> Johan Åqvist,<sup>†</sup> Nicholas H. Williams,<sup>\*,‡</sup> and Shina C. L. Kamerlin<sup>\*,†</sup>

<sup>†</sup>Department of Cell and Molecular Biology (ICM), Uppsala University, SE-751 24 Uppsala, Sweden

<sup>‡</sup>Department of Chemistry, Sheffield University, Sheffield, S3 7HF, U.K.

### Supporting Information

**ABSTRACT:** Understanding phosphoryl and sulfonyl transfer is central to many biochemical processes. However, despite decades of experimental and computational studies, a consensus concerning the precise mechanistic details of these reactions has yet to be reached. In this work we perform a detailed comparative theoretical study of the hydrolysis of *p*-nitrophenyl phosphate, methyl phosphate and *p*-nitrophenyl sulfate, all of which have served as key model systems for understanding phosphoryl and sulfonyl transfer reactions, respectively. We demonstrate the existence of energetically similar but mechanistically distinct possibilities for phosphate monoester hydrolysis. The calculated kinetic isotope effects for *p*-nitrophenyl phosphate provide a means to discriminate between substrate- and solvent-assisted pathways of phosphate monoester hydrolysis, and show that the solvent-assisted pathway dominates in solution. This preferred mechanism for *p*-nitrophenyl phosphate hydrolysis is difficult to find computationally due to the limitations of compressing multiple bonding changes onto a 2-dimensional energy surface. This problem is compounded by the need to include implicit solvation to at least microsolvate the system and stabilize the highly charged species. In contrast, methyl phosphate hydrolysis shows a preference for a substrate-assisted mechanism. For *p*-nitrophenyl sulfate hydrolysis there is only one viable reaction pathway, which is similar to the solvent-assisted pathway for phosphate hydrolysis, and the substrate-assisted pathway is not accessible. Overall, our results provide a unifying mechanistic framework that is consistent with the experimentally measured kinetic isotope effects and reconciles the discrepancies between theoretical and experimental models for these biochemically ubiquitous classes of reaction.



### ■ INTRODUCTION

The hydrolysis of phosphate esters plays a central role in many biological processes, including energy production, signal transduction, and maintaining the integrity of genetic material.<sup>1,2</sup> The rates of the uncatalyzed hydrolyses of these biochemically ubiquitous compounds are exceedingly slow,<sup>3,4</sup> with half-lives potentially in the trillions of years,<sup>3</sup> so the enzymes that catalyze these difficult reactions produce some of the largest known enzymatic rate enhancements.<sup>4,5</sup> In light of its biological importance, a considerable body of experimental and theoretical data aimed at understanding the details of this reaction has accumulated over the years (for detailed reviews, see refs 6 and 7 and references cited therein). However, despite these data, just how this reaction proceeds in solution and in enzyme catalyzed processes remains controversial.

Understanding phosphate ester hydrolysis is made complicated by the availability of multiple plausible mechanisms for the same reaction<sup>6,7</sup> (Figure 1). For example, in the case of phosphate monoester dianions, experimental evaluation of kinetic isotope effects,<sup>8</sup> linear free energy relationships<sup>9,10</sup> and entropic effects<sup>10</sup> have suggested that this reaction proceeds through a concerted pathway with a loose, metaphosphate-like transition state (TS) (in contrast to the more associative

transition states expected for the hydrolysis of phosphate di- and triesters, see discussion in ref 6). On the other hand, computational studies have suggested two viable concerted pathways with TSs that are either dissociative or associative in nature, and become looser or tighter depending on the  $pK_a$  of the leaving group.<sup>11–15</sup> Additionally, a number of computational studies have suggested the existence of both phosphorane<sup>16</sup> and metaphosphate<sup>17</sup> intermediates, and sometimes even multiple different mechanisms have been suggested for the same system.<sup>12,14,16–19</sup> Finally, it has been suggested that the qualitative interpretation of traditional experimental markers such as linear free energy relationships,<sup>12,18,20</sup> activation entropies<sup>14</sup> and isotope effects<sup>12</sup> can be ambiguous, with different pathways giving rise to similar experimental observables.<sup>18</sup>

A recent key point of discussion has revolved around deprotonation of the water nucleophile and the identity of the ultimate proton acceptor (see discussion in refs 6 and 7). This becomes a particularly important issue when dealing with enzyme-catalyzed phosphoryl transfer, where the identity of the

Received: August 12, 2014

Published: November 7, 2014

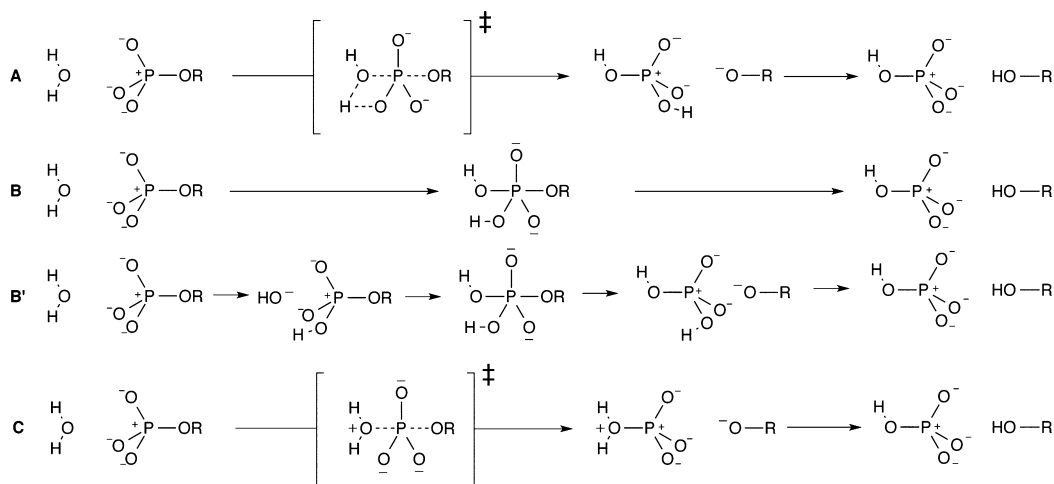


**Figure 1.** Hypothetical mechanisms for the hydrolysis of phosphate monoester dianions considered in this work. (A) Concerted mechanism with substrate-assisted nucleophilic attack, in which the attacking water molecule is deprotonated by the substrate at some point along the reaction coordinate. (B) Stepwise mechanism in which proton transfer from the nucleophile to the substrate, concerted with nucleophilic attack, leading to a pentacoordinate intermediate which breaks down with concerted proton transfer to the leaving group. (B') Stepwise mechanism in which the proton transfers precedes nucleophilic addition and follows leaving group departure. (C) Concerted mechanism with solvent-assisted nucleophilic attack, in which there is no proton transfer from the nucleophile in the rate-limiting step. Note that this figure is condensed for clarity; for considerations of microscopic reversibility, see the Supporting Information.<sup>24</sup>

general base is not immediately obvious. In principle, the reaction could proceed via a substrate-assisted mechanism in which the phosphate is the ultimate proton acceptor, and theoretical works have argued in favor of such a mechanism in the cases of, e.g., GTP hydrolysis by GTPases such as Ras<sup>21</sup> and the elongation factor thermounstable (EF-Tu) in complex with the ribosome.<sup>22</sup> However, not just the viability of such a mechanism has been debated,<sup>23</sup> but also, more recently, whether deprotonation of the nucleophile during bond formation to the phosphorus is necessary at all.<sup>6</sup>

Computational studies on the reaction in water have supported an important role for proton transfer from the incoming water nucleophile, either through a ground state pre-equilibrium proton transfer followed by hydroxide ion attack on a monoanionic phosphate monoester in the case of methyl phosphate hydrolysis,<sup>13,21</sup> or as a concerted process in the case of *p*-nitrophenyl phosphate hydrolysis.<sup>25</sup>

Phosphate monoester dianions are difficult to study experimentally due to the very low reactivity of these compounds.<sup>3</sup> As a result, aryl phosphate monoester dianions with good leaving groups, and especially *p*-nitrophenyl phosphate (*p*NPP),<sup>8–10</sup> have been used to understand this reaction because they react sufficiently rapidly to allow for detailed mechanistic analysis. Classically, their hydrolysis is described as proceeding through a loose dissociative transition state, based on a measured  $\beta_{\text{lg}}$  of  $-1.23$ ,<sup>9</sup> an inverse  $^{18}\text{k}_{\text{nonbridge}}$  isotope effect (0.9994) on the nonbridging oxygens of *p*NPP, a large normal isotope effect on the bridging oxygen to the *p*-nitrophenyl leaving group ( $^{18}\text{k}_{\text{bridge}} = 1.0189$ ), and a  $^{15}\text{k}$  isotope effect of close to the maximum that would be expected for breaking the bond to the leaving group at the transition state (1.0028).<sup>8</sup>

Despite the experimental importance of this system, theoretical studies on *p*NPP hydrolysis have been very limited, with only two studies on the hydrolysis of this compound (involving alkaline<sup>26</sup> and spontaneous<sup>25</sup> reactions), along with a study on the related aminolysis.<sup>27</sup> For the alkaline reaction, it should be noted that that phosphate monoester dianions are

extremely resistant to hydroxide attack, and in fact there is no evidence for hydroxide attacking the phosphorus of this or any other phosphate dianion.<sup>10</sup> For the spontaneous reaction, calculations provided the experimentally observed activation barrier of  $29.1 \text{ kcal}\cdot\text{mol}^{-1}$ <sup>10</sup> and suggested that the reaction proceeds through a single transition state with concerted proton transfer to the phosphate, consistent with previous theoretical studies of related compounds in aqueous solution.<sup>12</sup> These same methods were able to reproduce the similar activation barrier for *p*-nitrophenyl sulfate monoester<sup>28,29</sup> hydrolysis, and the rather large difference in activation entropy between the two reactions<sup>10,28</sup> However, two features stand out in these calculations.<sup>25</sup> First, the calculated energy landscape (Figure S1) did not provide a clear saddle point, but only a high-energy ridge along which the transition state was found. The second issue is that despite agreement with some of the experimental data, it was not possible to reproduce the kinetic isotope effects, even though good agreement was obtained for the kinetic isotope effects for the sulfate monoester analogue, suggesting that this is not a complete picture of the reaction.

To resolve the differences between experimental data and theoretical predictions, we have examined in detail the hydrolysis of three model compounds in aqueous solution: *p*-nitrophenyl phosphate (*p*NPP), methyl phosphate (MP) and *p*-nitrophenyl sulfate (*p*NPS) monoesters. In doing so, we can directly compare the hydrolysis of phosphate monoesters with both good (aryl) and poor (alkyl) leaving groups, as well as the hydrolysis of the corresponding arylsulfate monoester. This is particularly important in the case of methyl phosphate where both associative<sup>12</sup> and dissociative<sup>14</sup>  $\text{A}_{\text{N}}\text{D}_{\text{N}}$  mechanisms, as well as a stepwise mechanisms involving proton transfer to substrate<sup>16</sup> have been suggested as viable reaction pathways depending on the computational setup. In the latter case, these elegant calculations were computationally costly as they were performed in full explicit solvent. Therefore, it is useful to compare the effect of using an implicit solvent model and a small number of discrete water molecules with the calculations in explicit solvent to find out if a simpler and less costly

approach can provide comparable results. We demonstrate that including such microsolvation can substantially affect both the geometries and calculated activation barriers obtained for these species, but that the inclusion of even a few explicit water molecules allows the calculated energetics to converge within a range that would be expected from small variations in the positions of the water molecules. From these calculations, it can be seen that leaving group ability plays an important role not just in the choice of mechanism but also in the role of proton transfers in the reaction. The present work is also the only study to date that computationally reproduces the experimentally observed kinetic isotope effects for the hydrolysis of phosphate monoester dianions. Finally, we note the limitations of using calculated 2-dimensional More O'Ferrall Jencks plots<sup>30,31</sup> to deduce mechanistic conclusions for multidimensional systems. While they can be very powerful tools, without proper configurational sampling it is possible to lose the preferred reaction pathway from the calculated surface.

## METHODOLOGY

**Generating 2-D Energy Landscapes.** Two dimensional (2-D) energy surfaces for water attack on *p*NPP, MP and *p*NPS in the presence of two extra explicit water molecules were generated in the space defined by the phosphorus–oxygen distances to the departing leaving group (P–O<sub>lg</sub>, *x*-axis) and incoming nucleophile (P–O<sub>nuc</sub>, *y*-axis) using a grid of 0.1 Å increments, and mapping from 1.6 to 3.4 Å along each coordinate. At each point on this surface, the two relevant distances were kept fixed and all other degrees of freedom (including the proton of the attacking water molecule) were allowed to optimize. The energy landscapes were scanned in both the reactant-to-product and product-to-reactant directions in order to ensure that the true minimum energy surface was obtained.

Initial geometry optimizations were performed in the gas phase using the 6-31+G\* basis set, and the M06-2X functional,<sup>32</sup> followed by single point calculations on the structures obtained with a larger (6-311+G\*\*) basis set to obtain the final energy for each point (relative to the reactant complex). Solvation was primarily accounted for by the solvent model density (SMD) continuum solvent model,<sup>33</sup> with the inclusion of two additional explicit water molecules, one positioned to stabilize the leaving group and the other to stabilize the nucleophile. Including these water molecules allows comparison with the corresponding surfaces previously obtained for these compounds using a purely implicit solvation model.<sup>12,25</sup> Note that we refer to these surfaces as “energy landscapes” rather than potential or free energy surfaces because the solvation entropy is implicitly accounted for by the continuum model, but the configurational entropy is not. Despite this limitation, the 2-D surfaces provide initial insight into viable pathways and approximate locations of key stationary points which we then verified by unconstrained transition state optimizations and subsequent free energy corrections, as outlined below.

**Generating 1-D Free Energy Landscapes and Exploring the Role of Explicit Solvation.** In recent years, it has become increasingly popular to model phosphate and other group transfer reactions using a “mixed” solvation model in which the solvent is represented by an implicit model and a number of explicit water molecules (see refs 17, 26, 27, 34). Despite the technical limitations of such an approach,<sup>35</sup> this has been shown to be especially useful in reactions involving highly charged species, where the charge on the solute atoms is not properly solvated by the continuum model.<sup>36</sup> As the popularity of such mixed models increases, questions also arise about the extent to which the inclusion of explicit water molecules affects the energetics of the reaction and geometries of key stationary points, as well as the number of additional water molecules that are required before one obtains a stable, convergent result.

To explore these issues, we have considered two potential pathways for the nucleophilic addition of water to each of the substrates considered in this work (Figure 1). The first of these is a substrate-assisted mechanism in which nucleophilic attack occurs in either a

concerted fashion (Figure 1A) or via a metastable pentacoordinate intermediate (Figure 1B and 1B'). These are coupled with proton transfer from the attacking water molecule to one of the nonbridging oxygens of the phosphate, which can also be either stepwise (preceding nucleophilic attack) or concerted with nucleophilic attack. The second is a concerted mechanism in which the nucleophile is not deprotonated in the rate-limiting transition state (Figure 1C), but is stabilized by the solvent. The initial product of this reaction is expected to be only transiently stable (estimated  $pK_a \sim -5$ <sup>37</sup>), and to transfer a proton from the nucleophile to either solvent or to a more basic site via a chain of water molecules. These will be henceforth referred to as either substrate-assisted (Figure 1A and B) or solvent-assisted (Figure 1C) mechanisms, respectively.<sup>24</sup> In each case, the relevant transition states were optimized with no constraints at the M06-2X/6-31+G\*/SMD level of theory, using an ultrafine numerical integration grid. The resulting transition state was characterized by frequency calculations, as well as by following the intrinsic reaction coordinate (IRC)<sup>38,39</sup> to minima in both directions, followed by unconstrained geometry optimizations at the same level of theory. Additional single point frequency calculations (using a scaling factor of 0.970, by analogy to suggestions presented in related basis sets<sup>40</sup>) for the key stationary points were performed using the larger 6-311+G\*\* basis set to correct for zero-point energies and entropies and obtain the final free energies for these reactions. It should be noted that Alexeev et al.<sup>41</sup> have argued for the importance of using a larger basis set for polarizable atoms such as P and S if one wants to achieve near chemical accuracy in the thermodynamic properties for these compounds. In terms of the basis set dependence, it has been shown by Ribeiro et al. in their benchmark studies of phosphate diester hydrolysis<sup>42</sup> that this is an important aspect for the hydroxide reaction, but less so for the water reaction. These authors showed that basis sets including polarization and dispersion terms such as 6-311+G(d,p) can already provide accurate results (with MUE (mean unsigned error) of about 1.2–1.7 kcal/mol), no improvement was seen upon inclusion of a second diffuse function, and further reduction of MUE values was also obtained using the 6-311+G(2d,2p) basis set (which in the cited benchmark study led to a MUE of about 0.5 kcal/mol). In our case, moving to a larger (6-311+G(2d,2p)) basis set slightly affects the calculated energetics (by <1 kcal/mol), but does not change the trends in our calculations (Table S1). Activation free energies were obtained relative to the reactant complex state (RS); in cases where multiple pathways are accessible, the lowest energy RS was chosen as a reference for all pathways. (Tables S2–S6 contain the corrected and uncorrected activation and reaction energies.) This procedure was repeated for each system in the presence of 0–8 explicit water molecules, in addition to the nucleophile, with the aim of examining the effect of including explicit hydrogen bonding interactions in the system. To avoid biasing the position of the water molecules, each additional water molecule was alternately positioned so as to stabilize first the leaving group and then the nucleophile side of the phosphate, thus maintaining the system as symmetric as possible. All quantum chemical calculations were performed using the Gaussian09 simulation package.<sup>43</sup>

Finally, the semiclassical kinetic isotope effects (KIE) were evaluated directly from the vibrational frequencies using the Biegelsen–Mayer equation,<sup>44,45</sup> as implemented in Quiver.<sup>46</sup> Note that in the context of the entropy calculations, in principle, one needs to take into account the entropic contribution from the explicit water molecules. In a previous work<sup>25</sup> we examined both solvent and solute entropies using explicit molecular dynamics sampling for the solute entropies and obtained excellent agreement with experiment. However, the complexity associated with using such a protocol for the large number of systems examined in this work is prohibitive, and therefore, we have relied on estimates from the QM-calculated vibrational frequencies (which allowed us to compare different mechanistic possibilities for the same system).

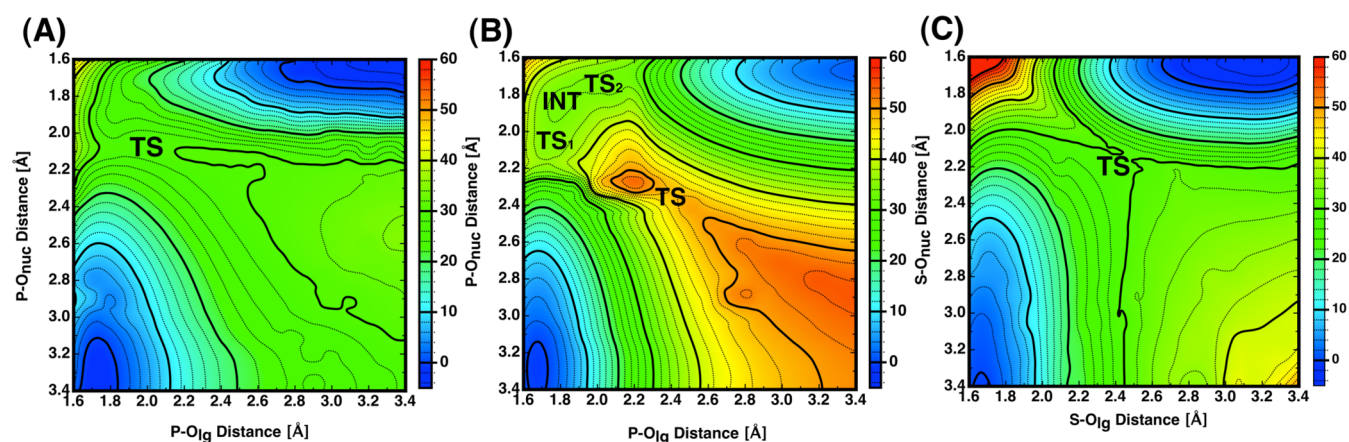


**Figure 2.** Calculated energy landscapes and approximate transition state positions (TS) for the hydrolysis of (A) *p*NPP, (B) MP, and (C) *p*NPS at the M06-2X/6-311+G\*\*(SMD)//M06-2X/6-31+G\*(gas) level of theory in the presence of two additional explicit water molecules. All energies are presented in kcal·mol<sup>-1</sup> relative to the reactant complex, and INT indicates the position of a metastable intermediate.

## RESULTS AND DISCUSSION

***p*-Nitrophenyl Phosphate Hydrolysis.** Given the unusual features of the previously reported energy landscape for *p*NPP (Figure S1 and ref 25), we have recalculated the energy landscape for this reaction in the presence of two extra explicit water molecules, as outlined in the Methodology section, to see if the surface can provide insight into which reaction pathways are likely to be viable for this system. The resulting energy landscape is shown in Figure 2A. It can be seen that allowing for microsolvation of the negative charge and using a dispersion-corrected functional qualitatively changes the landscape quite drastically, such that a clear saddle point can be observed. However, the position of the approximate transition state is virtually identical to that obtained from the calculations in implicit solvent without the dispersion correction,<sup>25</sup> and a substrate-assisted mechanism is again revealed by the energy landscape. Performing an unconstrained transition state optimization on this structure and following the IRC from this transition state to obtain reactant and product complexes resulted in a calculated activation barrier of 34.9 kcal·mol<sup>-1</sup>, which is very close to the value (33.0 kcal·mol<sup>-1</sup>) obtained in our previous work at a different level of theory with no extra explicit water molecules,<sup>25</sup> and within 5.4 kcal·mol<sup>-1</sup> of the experimental value of 29.1 kcal·mol<sup>-1</sup>.<sup>10</sup>

Further examination of the surface shown in Figure 2A suggests that the reaction has a single low energy pathway with a compact TS (P–O distances of 2.27 and 1.75 Å to the nucleophile and leaving group, respectively). As pointed out by a Reviewer, even though a stable intermediate is not apparent, the reaction pathway passes very close to the A<sub>N</sub> + D<sub>N</sub> corner of the diagram suggesting that an enforced concerted reaction may be an appropriate description. The energy contours near this corner (P–O distances of 1.9 and 1.8 Å to the nucleophile and leaving group, respectively) show a broadening which is the pattern expected for this mechanism, and which would deepen into a potential well for poorer leaving groups. In this description, the reaction is concerted because the potential phosphorane intermediate is not stable enough to exist, and the structural changes resemble those for forming a phosphorane rather than a synchronous reaction. This is similar to previous theoretical studies, but conflicts with the dissociative “expanded” transition state that is widely used to rationalize experimental data, and with the suggestion that deprotonation

of the nucleophile is not necessary in the rate-limiting step of the reaction.<sup>6</sup> Although an expansive TS is not evident from the surface, it was computationally observed for the analogous sulfate monoester<sup>25</sup> (also see below).

To test whether a similar TS is accessible for *p*NPP, we used the sulfate transition state as a starting point. This revealed another lower energy TS with P–O distances of 2.34 and 2.45 Å to the nucleophile and leaving group, respectively (Figure 3).

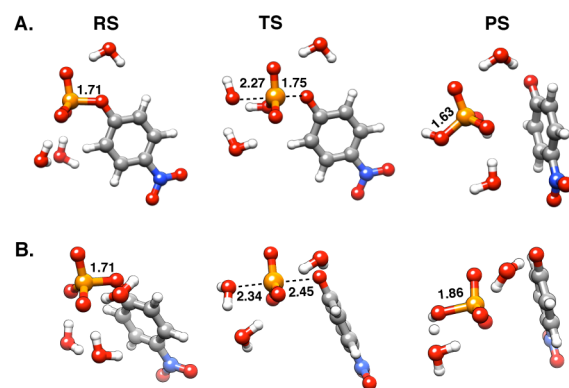


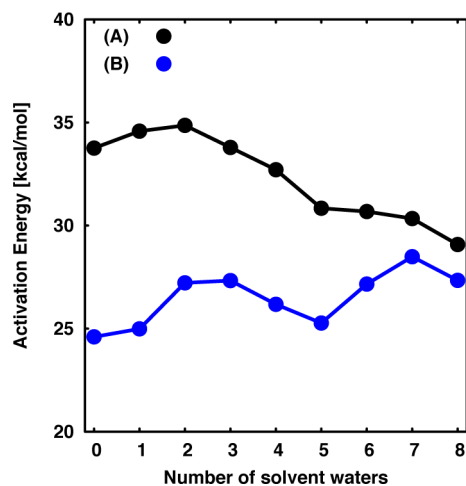
**Figure 3.** Representative stationary points for (A) substrate-assisted and (B) solvent-assisted hydrolyses of *p*NPP in the presence of two additional water molecules, as well as continuum solvent (SMD). RS, TS and PS denote reactant, transition, and product states, respectively. All distances are in Å.

This pathway appears to be preferred over the corresponding substrate-assisted pathway by 8 kcal/mol (Table S7 presents a summary of the energetics for the two different mechanisms). Following from this, to check whether the direct transfer of a proton from the nucleophile to the phosphoryl oxygen through a 4-membered ring provides an artificially high barrier for the substrate-assisted pathway investigated, we have also explored the effect of using one of the additional water molecules as bridge for the proton transfer. In the case of *p*NPP hydrolysis, the bridging water TS is slightly (0.8 kcal/mol) higher in energy than the TS for direct transfer. In both cases, we note that proton transfer has occurred before the TS is reached. Therefore, irrespectively of whether protonation of the phosphate occurs via an intervening water molecule or through

direct deprotonation of the nucleophile, the solvent assisted mechanism is still the preferred mechanism.

It is surprising that the energetically preferred mechanism appears to be absent from the energy surface shown in Figure 2A. To rationalize this, we note that in the solvent-assisted mechanism the nucleophile has not been deprotonated and the initial “product” state is a transient species with an elongated bond to the incoming nucleophile (Table S8). This will have a very short lifetime as the nucleophile is rapidly deprotonated and the P–O<sub>nuc</sub> bond subsequently compresses. The pathway to this species is overwhelmed by the exothermicity of the proton transfer involved in the substrate-assisted mechanism when calculating the surface shown in Figure 2A, causing it to artificially vanish from the 2-D surface. Specifically, the 2-D surface is a projection in which each point corresponds to only two fixed distances with multiple conformations satisfying these criteria. Therefore, the system will always try to find the lowest energy structure even if this is not directly connected to the lowest energy transition state, creating hysteresis on the surface. The O–H distances on the attacking water molecule can be constrained to prevent proton transfer to the phosphate and enforce a solvent-assisted mechanism, and such a surface for *p*NPP hydrolysis is shown in Figure S2. However, completely preventing the proton transfer results in an energy landscape in which the transition state all but vanishes, and represents entry to the bottom of a high energy valley on the potential surface that describes the product state (as this constraint prevents transfer to solvent or to the phosphate late in the reaction). Therefore, this landscape is only informative near the transition state. This highlights the danger of reducing a complex multidimensional reaction pathway to a simple two-dimensional geometric representation (see also refs 47 and 48), despite the usefulness of such surfaces when studying less complex systems.

To take into account the effect of the explicit water molecules, we repeated the transition state optimization by including 0–8 extra water molecules in the calculation. A comparison of the energetics between the solvent- and substrate-assisted pathways with an increasing number of explicit water molecules is presented in Figures 4 and S3 and Table S7, with the corresponding energy breakdowns shown in



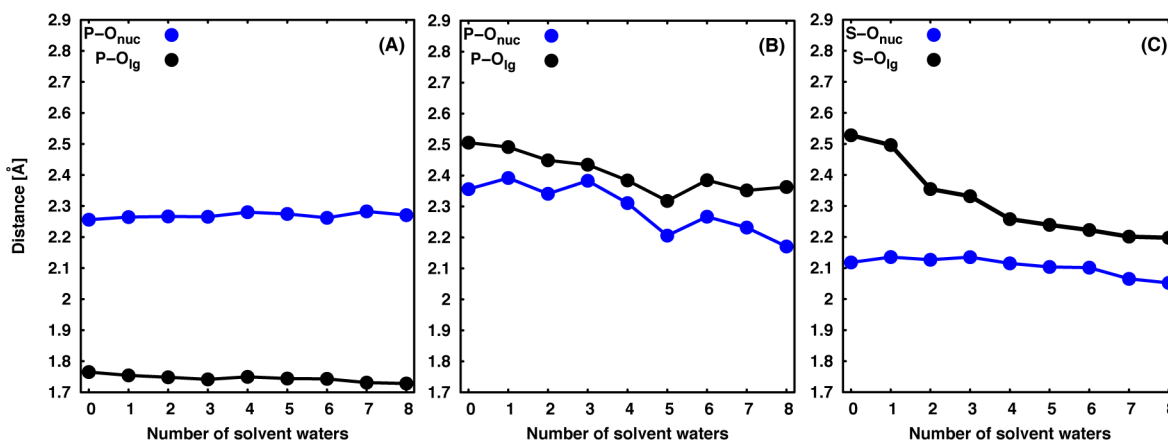
**Figure 4.** Change in activation barriers for (A) substrate-assisted and (B) solvent-assisted mechanisms for the hydrolysis of *p*NPP upon adding an increasing number of water molecules to the calculation.

Table S2 and S3. From these data, it can be seen that including extra explicit water molecules has a substantial effect on the calculated activation barrier, with each extra water molecule lowering the calculated activation barrier for the substrate-assisted mechanism, presumably due to better solvation of the TS by introducing explicit hydrogen bonding interactions. Even after including 8 explicit water molecules, the calculations do not appear to be fully converged, although they appear to be close to that point. However, the TS optimizations and more problematically the subsequent IRC calculations become computationally costly and so we did not add further water molecules. With enough explicit water molecules, it appears that the energies of the two pathways converge such that they are similar to each other (Figure 4).

Interestingly, while the energetics of the substrate-assisted reaction appear to be substantially affected by the inclusion of the water molecules, the corresponding effect on the transition state geometries is small (Figure 5A and Table S8), and therefore the origin of the decreasing activation barrier is not structural but due to the energetic consequences of explicit H-bonding interactions introduced by the added water molecules. In contrast, adding an increasing number of explicit water molecules to the solvent-assisted reaction gradually tightens the transition state by up to 0.2 Å in the bond lengths to the nucleophile or leaving group (Figure 5B and Table S8). However, this still corresponds to very little bond order to either nucleophile or leaving group at the transition state. Specifically, the Wiberg bond index of the forming P–O<sub>nuc</sub> bond is 0.11 and breaking P–O<sub>lg</sub> is 0.08 (see Figure S4 for a comparison of the bond index at the TS for the different pathways). Figure 4 (as well as Figure S3 and Table S7) shows that in the presence of no additional water molecules, the dissociative (solvent-assisted) pathway is initially energetically favorable over the associative (substrate-assisted) pathway by 9.2 kcal·mol<sup>-1</sup>, but this drops to 2 kcal·mol<sup>-1</sup> upon adding eight explicit water molecules, as the transition state for the substrate-assisted pathway is more stabilized upon adding explicit microsolvation.

That is, adding extra water molecules causes the calculated activation barriers for the solvent-assisted mechanism to fluctuate over a 4 kcal·mol<sup>-1</sup> range, giving an average activation barrier of 26.5 ± 1.3 kcal·mol<sup>-1</sup> over all combinations of explicit water molecules tested in this work. This is about 3 kcal·mol<sup>-1</sup> lower than the experimental value of 29.1 kcal·mol<sup>-1</sup> at 25 °C.<sup>10</sup> However, our QM calculations probably underestimate the solvation of the charged species in the ground state, so the calculated activation barrier can be considered a lower limit.

It is clear that the two pathways have somewhat different geometries. One feature is that the hydrogen atoms of the nucleophilic water are either stabilized by the microsolvation, leading to the solvent-assisted transition state, or interact with a nonbridging oxygen of the phosphate, leading to the substrate-assisted transition state. Thus, one difference between the pathways appears to be the capacity to trap the acidic hydrogen with the phosphoryl group. Less obviously, the preferred position of the aromatic ring relative to the scissile bond is different. Here, there are two possible conformations depending on whether the scissile bond is coplanar with or perpendicular to the aromatic ring, with the phosphoryl group either moving away from or over the aromatic ring as the reaction proceeds (Figure S5). For the substrate-assisted pathway, the scissile bond is preferentially coplanar with the aromatic ring at the transition state (Table S2). In fact, TSs for



**Figure 5.** Variation in P/S–O<sub>nuc</sub> and P/S–O<sub>ig</sub> distances at the transition state upon adding an increasing number of water molecules to the calculation for the (A) substrate- and (B) solvent-assisted spontaneous hydrolyses of *p*NPP, as well as (C) the solvent-assisted spontaneous hydrolysis of *p*NPS.

the perpendicular conformation are only accessible once three or more water molecules have been added to the system, and then with energy differences of up to 4 kcal·mol<sup>-1</sup> between the two conformations (Table S2).

In contrast, for the solvent-assisted pathway, this discrimination is not apparent. The conformation in which the scissile bond is approximately perpendicular to the aromatic ring is the same energy within error as the coplanar conformation (Table S3). Thus, the conformational effect appears to be more important for the substrate-assisted pathway. Interestingly, for *p*NPS, there is a preference for the perpendicular conformation (obtaining the coplanar conformation was extremely difficult and only possible for a few cases, see below). This leads to different stereoelectronic features for the two mechanisms.

For the substrate-assisted pathway, if the scissile bond is coplanar with the aromatic ring, conjugation into the aromatic ring is present during bond cleavage (which is not far advanced at the TS). For the solvent-assisted pathway, the scissile bond is largely broken at the TS and so the increasing charge density at the leaving oxygen atom can be stabilized by the aromatic ring in both conformations (Table S9). The barrier to rotation in the ground state is only 2 kcal·mol<sup>-1</sup> (Figure S5), and inspection of the Cambridge Crystallographic database<sup>49</sup> reveals that the major populations of the P–O–C–C dihedral angle are centered around either 0 or 90°, therefore both conformations seem to be readily populated. This suggests that there may be an element of conformational control that could dictate which pathway is favored. Clearly, these observations only have potential relevance for aryloxy leaving group, and cannot be readily extended to alkyl phosphates or phosphate anhydrides.

We note that when comparing the energetics of the two different pathways, the reactant state should be the same regardless of the mechanism followed. In the present case, we have followed the minimum energy pathway that connects the respective reactant and transition state for each mechanism, but used the same (lowest energy) RS as a reference for the two different pathways/ring orientations. However, for comparison, in Table S2 and S3 we also present the energetics obtained using the RS from following the IRC for each mechanism and conformation. The use of a unique reference RS for the each mechanism does not change the overall trends nor the fact that the dissociative mechanism appears to be the favored pathway

up until 7 or 8 water molecules are present where the difference between the two pathways becomes smaller (see Figure 4).

Having analyzed the energetics of both pathways, both mechanisms appear plausible within the tolerance of the methods employed, and thus the relative energetics are inconclusive. The experimentally observed kinetic isotope effects (KIEs) remain to be accounted for and might be used to distinguish between the two pathways.

In our previous work,<sup>25</sup> we were unable to reproduce the KIEs for *p*NPP hydrolysis, following the substrate-assisted mechanism, despite being able to reproduce the KIEs for *p*NPS hydrolysis, which followed a solvent-assisted, dissociative mechanism. We assumed that this was because of complications due to the proton transfer and the fact that such isotope effects are rather difficult to calculate. In the present work, we have calculated KIEs for both the substrate-assisted and solvent-assisted transition states using the Biegeleisen-Meyer<sup>44</sup> equation as outlined in Methodology section. The resulting KIEs are shown in Table 1.

As with our previous work,<sup>25</sup> the calculated KIEs for the substrate-assisted mechanism give rather poor agreement with experiment, despite this pathway appearing energetically plausible as long as sufficient explicit water molecules are included. In each case, the KIE is very close to 1, and qualitatively wrong for the <sup>18</sup>k<sub>bridge</sub> KIE. The same outcome is obtained when the proton transfer occurs via a bridging solvent molecule (Table S10), with the calculated KIE still giving very poor agreement with experiment. In contrast, the calculated KIEs for the solvent-assisted mechanism give much better agreement with experiment, albeit with slightly overestimated values for the <sup>18</sup>k<sub>bridge</sub> KIE, and particularly good agreement for the <sup>15</sup>k KIE. The calculated KIEs are also very stable once two or more water molecules are added to the system and are apparently not affected by the extra degrees of freedom being introduced.

While quantitative accuracy have been reported for the alkaline hydrolysis of phosphate diesters,<sup>50</sup> this is, to the best of our knowledge, the first time it has been possible to theoretically reproduce the experimental KIEs for the spontaneous hydrolysis of phosphate monoesters, via a pathway normally not considered theoretically. An earlier study on the hydrolysis of *p*NPP assuming general base catalysis by a hydroxide ion obtained reasonable values for all KIE except for the <sup>18</sup>k<sub>nonbridge</sub>, which was qualitatively wrong.<sup>26</sup> Overall, the

Table 1. Comparison of the Calculated and Experimental  $^{18}k_{\text{bridge}}/^{18}k_{\text{nonbridge}}$  and  $^{15}k$  KIEs for *p*NPP and *p*NPS Hydrolysis<sup>a</sup>

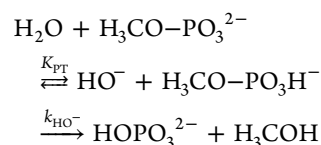
| #                   | <i>p</i> NPP <sup>b</sup>        |                        |                                 |                             | <i>p</i> NPS <sup>c</sup>       |                             |                             |                        |
|---------------------|----------------------------------|------------------------|---------------------------------|-----------------------------|---------------------------------|-----------------------------|-----------------------------|------------------------|
|                     | associative (substrate assisted) |                        | dissociative (solvent assisted) |                             | dissociative (solvent assisted) |                             | $^{15}k$                    |                        |
|                     | $^{18}k_{\text{bridge}}$         | $^{15}k$               | $^{18}k_{\text{bridge}}$        | $^{18}k_{\text{nonbridge}}$ | $^{18}k_{\text{bridge}}$        | $^{18}k_{\text{nonbridge}}$ | $^{18}k_{\text{nonbridge}}$ | $^{15}k$               |
| 0                   | 0.9703                           | 1.0003                 | 1.0290                          | 0.9974                      | 1.0045                          | 1.0316                      | 0.9940                      | 1.0064                 |
| 1                   | 0.9983                           | 1.0003                 | 1.0253                          | 0.9973                      | 1.0037                          | 1.0280                      | 0.9939                      | 1.0053                 |
| 2                   | 0.9981                           | 1.0001                 | 1.0312                          | 0.9966                      | 1.0036                          | 1.0260                      | 0.9947                      | 1.0044                 |
| 3                   | 0.9975                           | 0.9998                 | 1.0251                          | 0.9966                      | 1.0029                          | 1.0239                      | 0.9947                      | 1.0033                 |
| 4                   | 0.9973                           | 0.9996                 | 1.0266                          | 0.9962                      | 1.0025                          | 1.0182                      | 0.9945                      | 1.0037                 |
| 5                   | 0.9968                           | 0.9997                 | 1.0234                          | 0.9965                      | 1.0025                          | 1.0228                      | 0.9951                      | 1.0029                 |
| 6                   | 0.9964                           | 0.9995                 | 1.0234                          | 0.9960                      | 1.0026                          | 1.0218                      | 0.9953                      | 1.0028                 |
| 7                   | 0.9960                           | 0.9997                 | 1.0230                          | 0.9957                      | 1.0023                          | 1.0216                      | 0.9953                      | 1.0028                 |
| 8                   | 0.9959                           | 0.9996                 | 1.0254                          | 0.9954                      | 1.0025                          | 1.0241                      | 0.9938                      | 1.0040                 |
| average             | 0.9941 ± 0.0090                  | 0.9927 ± 0.0078        | 1.0258 ± 0.0027                 | 0.9964 ± 0.0007             | 1.0030 ± 0.0008                 | 1.0242 ± 0.0039             | 0.9946 ± 0.0006             | 1.0040 ± 0.0012        |
| exp <sup>d,28</sup> | <b>1.0189 ± 0.0005</b>           | <b>1.0028 ± 0.0002</b> | <b>1.0189 ± 0.0005</b>          | <b>0.9994 ± 0.0005</b>      | <b>1.0028 ± 0.0002</b>          | <b>1.0210 ± 0.0010</b>      | <b>0.9951 ± 0.0003</b>      | <b>1.0026 ± 0.0001</b> |

<sup>a</sup>In all cases the reactant state from the system without extra water molecules was used as the reference reactant state. Note that similar calculated KIE were obtained when using the reactant state from the IRC optimization as a reference point, and therefore, the qualitative results are independent of reference reactant state. <sup>b</sup>Calculated at 368 K (95 °C). <sup>c</sup>Calculated at 358 (85 °C). <sup>d</sup>28

system shows a preference for a dissociative pathway in which deprotonation of the nucleophile plays a marginal role with no need for general-base catalysis, although the corresponding substrate-assisted mechanism is sufficiently close in energy that an enzyme or synthetic catalyst could change the mechanistic preference of the system.

**Methyl Phosphate Hydrolysis.** Detailed experimental studies on phosphate monoester hydrolysis have mostly focused on the reactivity of arylphosphate monoesters,<sup>8–10</sup> with alkylphosphate monoesters much less studied due to their exceedingly slow rates: for example, the methyl phosphate dianion has an estimated rate constant of  $2 \times 10^{-20} \text{ s}^{-1}$  at 25 °C.<sup>3</sup> This estimate is an upper limit, as the reactivity of the monoanion dominates the observed reaction even in 1 M KOH. However, based on the similarity of estimates from these data with that obtained from an extrapolation of the Bronsted plot for the hydrolysis of arylphosphate monoester dianions,<sup>3,9</sup> it has been suggested that both alkyl and aryl compounds follow a similar mechanism.<sup>51</sup> Theoretical work has generally (with a few exceptions<sup>25–27</sup>) focused on the reactivity of phosphate monoesters with alkyl leaving groups,<sup>12–17,52–55</sup> and computational studies have been highly contradictory concerning the nature of this mechanism. That is, both stepwise<sup>15</sup> and concerted,<sup>12,14,53</sup> as well as associative<sup>12,53</sup> and dissociative<sup>14</sup> pathways have been suggested depending on the level of theory and computational approach used, and it has been suggested that the associative and dissociative pathways may be indistinguishable<sup>13,14,16</sup> by the available experimental methods.<sup>18</sup>

A particular point of discussion has been the importance of the potential proton transfer from the attacking nucleophile to the nonbridging phosphoryl oxygens. Specifically, there has been considerable discussion in the literature<sup>12,14,15,18,23,55</sup> about the viability of a substrate-assisted mechanism in which the phosphate itself deprotonates the attacking nucleophile in a pre-equilibrium proton transfer, which is followed by hydroxide attack on a protonated phosphate:



The key argument against such a mechanism is that the expected high cost of a ground state proton transfer from water to the phosphate (due to the large difference in  $\text{p}K_{\text{a}}\text{s}$ ) would require the subsequent nucleophilic attack of hydroxide on the phosphate monoanion to be extremely fast, far faster than the rate of reaction with a corresponding diester.<sup>23</sup>

Computational studies using methyl phosphate as a model system and implicit solvation have suggested such a mechanism is viable.<sup>55</sup> In contrast, studies of the alkaline hydrolysis of aryl alkyl phosphate diesters in which a methyl group is used as an analogue for a protonated phosphate have suggested that the rate of this reaction is far too slow to compensate for the low concentration of this ionic form.<sup>23</sup> However, and as also pointed out by Vigroux and co-workers,<sup>15</sup> it is not clear that methyl phosphate hydrolysis proceeds through a similar mechanism to an aryl phosphate with a good leaving group, particularly in light of the potential importance of leaving group protonation. Additionally, these arguments do not take into account the alternate possibility of a much later proton transfer to the phosphate that is concerted with or following bond

formation to the nucleophile rather than driving the reaction, as was suggested by calculations in full explicit solvation.<sup>16</sup> We also note that in a related study of phosphate diester hydrolysis, stepwise and concerted pathways had very similar activation energies.<sup>56</sup> In the case of *p*NPP we find that once sufficient water molecules are added to the system, both associative and dissociative pathways become comparable in energy. We have performed an analogous assessment of the hydrolysis of MP, although in this case there is almost no experimental data available for validation of the calculations, and therefore we provide only a theoretical model.

The energy landscape for the hydrolysis of this compound in the presence of two additional explicit water molecules is shown in Figure 2B. As with our previous work using a different density functional in pure implicit solvent,<sup>14</sup> two pathways are apparent on the energy landscape: an  $A_N + D_N$  associative pathway with concerted proton transfer to the phosphate during the addition step and a concerted pathway involving solvent-assisted water attack. However, the solvent-assisted transition state is at least 10 kcal·mol<sup>-1</sup> higher in energy than its substrate-assisted counterpart. As for *p*NPP, we explored whether the presence of an intervening water molecule significantly lowered the energy of the pathway involving proton transfer from nucleophile to phosphoryl oxygen (Table S11). The TS only differ by 0.3 kcal mol<sup>-1</sup>. As deprotonation of the nucleophile once again occurs prior to the TS (Figure S6), one would expect the TS for direct proton transfer and via water to have similar energetics as a 4-membered ring with shortened bonds between the hydrogen and the donor/acceptor sites is not evident in the TS. Although this pathway is not based on pre-equilibrium proton transfer, the TS is essentially the same as would be expected for this mechanism (see discussion below concerning reversibility).

A comparison between the energetics of the solvent- and substrate-assisted pathways with increasing number of solvent water is presented in Figure 6 (see also Figure S7). Once again, addition of extra explicit water molecules has a substantial effect on the calculated energetics, but in this case reducing the calculated activation barrier for the solvent-assisted pathway by up to 6 kcal·mol<sup>-1</sup>, while having a comparatively small effect on

the corresponding substrate-assisted pathway (see also Tables S4 and S5 for the breakdown of the different energy contributions) with almost no changes in TS geometries (Table S12 and Figure S8).

Performing the calculations in a pure implicit solvent model shows a substantial discrimination between the two pathways. However, once again, the introduction of explicit microsolvation by the addition of a sufficient number of explicit water molecules leads to a smaller energy difference between them (Figure 6 and Table S4 and S5), although preference for the substrate-assisted mechanism is still observed (previous studies have suggested similar energetics for both pathways<sup>13,16</sup>).

Key distances of the stationary points for the two different mechanisms are shown in Figure 7 and S9. The variation of the

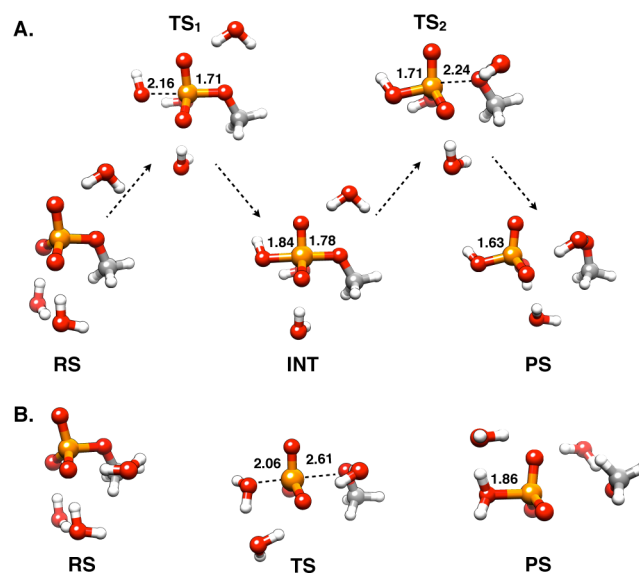


**Figure 7.** Representative stationary points for (A) stepwise substrate-assisted and (B) solvent-assisted hydrolyses of MP in the presence of two additional water molecules, modeled using continuum solvent (SMD). RS, TS, TS<sub>1</sub>/TS<sub>2</sub>, INT and PS denote reactant, transition states, intermediate, and product states, respectively. All distances are in Å.

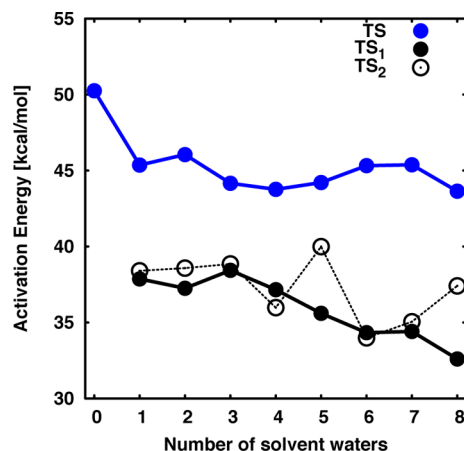


**Figure 6.** A comparison of the transition state energies for the spontaneous hydrolysis of MP upon adding an increasing number of water molecules to the calculation. Here, TS is the transition state for the solvent-assisted pathway, TS<sub>1</sub> is the transition state for the addition step of the substrate-assisted pathway, and TS<sub>2</sub> is the transition state for the elimination step of the substrate-assisted pathway.

relevant distances at the transition state, with an increasing number of water molecules, is shown in Figure 8 (and Figure S8 and Table S12), as can be seen the distances are more sensitive to the number of extra explicit water molecules for the solvent-assisted pathway compared to the substrate-assisted one.

In pure implicit solvent, the solvent assisted pathway would appear to be extremely unfavorable, with an activation barrier of 50.3 kcal·mol<sup>-1</sup>, although this is reduced to ~44 kcal·mol<sup>-1</sup> upon adding extra water molecules. As with the corresponding mechanism for *p*NPP hydrolysis, the “product” state is a high-energy metastable species with an elongated P–O<sup>+</sup>H<sub>2</sub> bond, prior to deprotonation of the nucleophile either by deprotonation to bulk water or tautomerization. This high energy species is expected to rapidly decay to a more stable product with a deprotonated nucleophile and a protonated leaving group, but we have not explored this outcome in detail as it is computationally challenging to model and not rate-limiting (note that in cases where the leaving group is protonated in the product state during the IRC or subsequent optimization, the energy drops dramatically; see Figure S7).

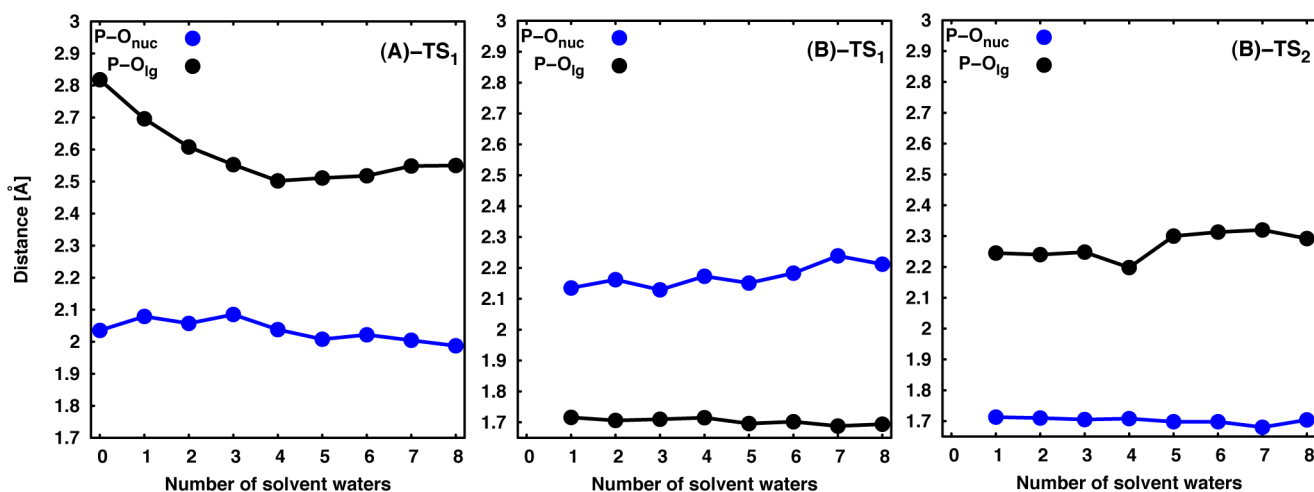


**Figure 8.** Variation in P–O<sub>nuc</sub> and P–O<sub>lg</sub> distances at the transition state upon adding an increasing number of water molecules to the calculation for the (A) solvent-assisted and (B) substrate-assisted (stepwise) hydrolyses of methyl phosphate (MP).

A slightly different mechanistic picture is obtained in the case of the substrate-assisted pathway, where the benefit of protonating the poor leaving group appears to provide a role for the formation of a transient phosphorane intermediate, with the proton of the nucleophile moving to a nonbridging oxygen of the phosphate. Examination of the individual points along the IRC suggests that this proton transfer occurs prior bond formation to the nucleophile. This is further validated by the analysis of both O–H and P–O distances along the reaction coordinate for both *p*NPP and MP systems (Figure S8). The structures of key stationary points along this pathway (corresponding to the surface shown in Figure S6), for the representative case with two extra water molecules, are shown in Figure 7. As can be seen from this figure, in the intermediate state, the proton on the nonbridging oxygen of the phosphate is still oriented toward the oxygen of the nucleophile, and for this proton to potentially protonate the leaving group, it first needs to rotate toward the oxygen of the leaving group. Schlitter and co-workers performed related calculations in explicit solvent<sup>16</sup> and obtained an estimated activation barrier of about 8 kcal·mol<sup>−1</sup> for this proton rotation. Consistent with these data, we were able to obtain transition states for this proton rotation in almost all cases, with approximate activation barriers of 4–6 kcal·mol<sup>−1</sup> (depending on how many extra water molecules are included in the system, cf. Table S6 and Figure S7).

Corresponding 1-D free energy profiles for both substrate-assisted and solvent-assisted pathways in the presence of eight additional explicit water molecules are shown in Figure 9. For the substrate-assisted mechanism, once the addition step has taken place, two different pathways can be followed. In the first of these (red), the P–OH of the intermediate phosphorane rotates to point the proton to the leaving group instead of the nucleophile, with a separate activation barrier to proton rotation (TS<sub>rot</sub> in Figure 9), followed by subsequent elimination of methanol. In the second, the breakdown of the phosphorane intermediate occurs through the elimination of an anionic (methoxy) leaving group (blue). As can be seen from Figure 9, these two scenarios are energetically indistinguishable, with the only difference that the rate limiting step changes from leaving group elimination to P–OH rotation giving essentially no added benefit from rotating this hydrogen to protonate the leaving group at the transition state. Once the proton rotation has occurred, leaving group departure becomes slightly easier

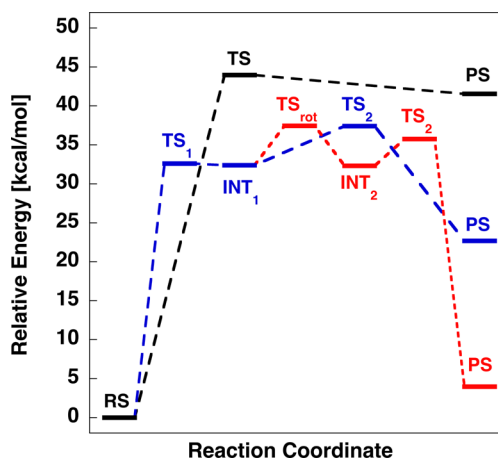


**Figure 9.** Calculated free energy profiles for methyl phosphate hydrolysis via different mechanisms in the presence of eight additional water molecules. Black: solvent-assisted; blue: substrate-assisted with elimination of methoxide; red: substrate-assisted with elimination of methanol following rotation of POH in phosphorane intermediate.

than the corresponding reaction without the proton rotation (Table S6 and Figure S7). Note that only the pathway involving rotation of the P–OH is compatible with microscopic reversibility. Expulsion of methoxide would mean that decomposition of INT1 does not mirror its formation, and would require an alternative mechanism for the formation of INT1 which involves the attack of hydroxide on the monoanion (with the P–OH oriented toward the leaving group; see Figure S9). However, it is apparent that the TS for the decomposition of both pathways from INT1 have similar energies, and so the additional pathway does not change the key aspects of the mechanism. Likewise, the solvent-assisted pathway has to have an alternative pathway where hydroxide attacks MP protonated on the leaving group to obey microscopic reversibility.

Finally, experimentally, the hydrolysis of MP is slightly exergonic, whereas our calculations show a slight endergonicity for the substrate-assisted pathway that leads to methanol as the initial product (PS3) and a very endergonic process for the solvent-assisted (PS1) and substrate-assisted pathways (PS2) that eliminate methoxide. The slightly endergonic substrate-assisted reaction is in part due to shortcomings of the implicit

solvent model, which undersolvates methanol relative to water, introducing an approximate error of 2.2 kcal/mol into the calculated endergonicity (see the discussion in the Supporting Information). It is possibly that an underestimate exists in the change in solvation free energy upon moving from methyl phosphate to inorganic phosphate. In addition, elimination of methoxide is expected to lead to a transient, high-energy intermediary state that rapidly decays to more stable products through proton transfers that are not rate limiting. There is a high endergonicity associated with modeling anionic species that has been particularly well documented in the case of reactions involving hydroxide-anion as a nucleophile (see discussion in refs 42 and 57). These problems result in artificial undersolvation of the anion, which in the case of hydroxide anion as a nucleophile leads to unphysically low activation energies (see discussion in our previous work<sup>47,57</sup>), and in the present case most likely leads to additional artificially high endergonicity for the departure of methoxide compared to methanol (a more detailed discussion of this issue is presented in the Supporting Information). Figure 9 shows a difference of 18.7 kcal mol<sup>-1</sup>, corresponding to a 14 pK<sub>a</sub> unit difference, which reflects the difference in pK<sub>a</sub> of methanol and the second ionization of inorganic phosphate; this should be only 9 pK<sub>a</sub> units. In contrast, the energy difference between the solvent- and substrate-assisted reactions that release methoxide is in good agreement with the estimated pK<sub>a</sub> difference between the two tautomers of monoanionic inorganic phosphate (~13 pK<sub>a</sub> units). As with our previous work,<sup>57</sup> we expect these problems to be mitigated at the TS, where there is partial bond formation to both incoming nucleophile and departing leaving group, allowing for meaningful trends to be obtained despite the uncertainties in the energetics of the product state.

***p*-Nitrophenyl Sulfate Hydrolysis.** In recent years, it has been convincingly demonstrated that a large number of enzymes are capable of “catalytic promiscuity” in that they can facilitate the turnover of multiple substrates through chemically distinct transition states.<sup>58</sup> This phenomenon has been particularly well described in enzymes that catalyze phosphoryl transfer reactions, with phosphatases multitasking as sulfatases and sulfatases multitasking as phosphatases (see refs 59–62 and references cited therein).

To understand such promiscuity, it is important to understand the intrinsic reactivity of these compounds, so that the origins of any potential changes in how different transition states are recognized can be mapped, and substantial effort has been made in this direction,<sup>25,57,63,64</sup> and how similar or different the intrinsic chemistry of aryl phosphate and sulfate hydrolysis actually is. Both *p*NPP and *p*NPS have similar (tetrahedral) ground state geometries, and similar experimentally measured rate constants<sup>10,28</sup> and KIEs<sup>8,28</sup> for their spontaneous hydrolysis. As a result, it has been assumed that these reactions proceed through very similar (dissociative) transition states. However, the two compounds differ by a full charge unit (resulting in potentially very different solvation effects at the transition state), and have very different experimentally measured activation entropies: -18.5 eu for the pH independent hydrolysis of *p*NPS anion<sup>29</sup> and +3.5 eu for the hydrolysis of *p*NPP dianion.<sup>10</sup>

A major difference between *p*NPP and *p*NPS is the acidity of the substrate: the second pK<sub>a</sub> of *p*NPP is ~4.9,<sup>65</sup> whereas *p*NPS has a pK<sub>a</sub> of < -3.<sup>66</sup> Therefore, a mechanism involving initial proton transfer to the substrate is much less favorable for the sulfate. Similarly, the product inorganic phosphate has a second

pK<sub>a</sub> of 6.82,<sup>5</sup> whereas inorganic sulfate has a first pK<sub>a</sub> of -3.0<sup>67</sup> and so there is no benefit for concerted proton transfer to the sulfate either. As can be seen from Figure 2C, the surface suggests only a single pathway, involving an expanded transition state with S–O distances of approximately 2.2 and 2.4 Å to the nucleophile and leaving group oxygen atoms respectively (similarly to our previous energy landscape<sup>25</sup>). Adding extra water molecules does slightly tighten this transition state (Figure 5C and Table S13), and also reduces the calculated activation barrier (Table S14 and Figure S11). In most cases, the product state still passes through a high-energy plateau, where the nucleophilic water molecule has now been deprotonated to yield a hydronium, hydrogen sulfate, and the aryloxy leaving group (as well as any extra water molecules). This hydronium ion ultimately protonates the leaving group, and the stability of the product state obtained from following the IRC appears to depend on the position of this hydronium ion, as shown in Figure 10. In contrast, for *p*NPP, the water

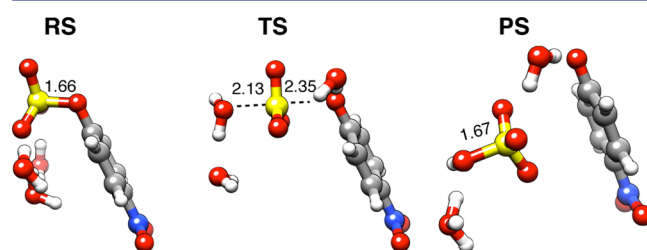


**Figure 10.** Representative stationary points for the solvent-assisted hydrolysis of *p*NPS in the presence of two additional water molecules, modeled using continuum solvent (SMD). RS, TS and PS denote reactant, transition, and product states, respectively. All distances are in Å.

molecule is not deprotonated at this inflection point on the reaction profile (for the solvent-assisted pathway), despite the similarity between the two transition states.

It should be noted that the *p*NPS transition state obtained from the surface shown in Figure 2C was crucial for locating the dissociative *p*NPP transition states shown discussed above. That is, all our prior attempts to optimize this transition states directly in pure implicit solvent resulted in decomposition of the phosphate to metaphosphate, water and *p*-nitrophenoxide (the optimization never converged), whereas it was possible to directly optimize the *p*NPP transition state shown in Figure 3 using the *p*NPS transition state presented here as a starting point. It should be noted that similar problems in obtaining TS for the hydrolysis of the sulfate monoester have also been recently reported.<sup>64</sup> Table 1 shows the calculated isotope effects at 85 °C, demonstrating that, as with our previous work,<sup>25</sup> we are able to obtain good agreement with experiment for this pathway even if the <sup>15</sup>k effect is slightly overestimated.

We also explored the potential substrate-assisted mechanism, but the calculated activation barriers lay in the range of ~50 kcal·mol<sup>-1</sup> (even after adding extra water molecules for explicit microsolvation), and so this mechanism was discounted as being too energetically unfavorable. Therefore, in contrast to the picture previously given by theory,<sup>25</sup> the “hidden” (but preferred) mechanism for *p*NPP hydrolysis and that for *p*NPS hydrolysis are very similar and proceed through very similar transition states, as has been inferred from the experimental data.<sup>8,28,68</sup> The main difference is that in the case of *p*NPP, there appears to be a second energetically similar pathway that

is accessible and either an artificial or biological catalyst, depending on the local electrostatic environment, might shift the balance between these two mechanisms. This is not possible for *p*NPS hydrolysis, where the substrate-assisted mechanism is extremely unfavorable and an external proton acceptor is always required. These results may provide insight into why it is apparently much harder for a proficient phosphatase to be also a good sulfatase (alkaline phosphatase (AP)<sup>69,70</sup>) than the other way around (e.g., *Pseudomonas aeruginosa* arylsulfatase (PAS)<sup>71</sup>).

## OVERVIEW AND CONCLUSIONS

In the current work, we present a detailed theoretical study of the hydrolysis of three representative model compounds, namely methyl phosphate hydrolysis, *p*-nitrophenyl phosphate hydrolysis and, for comparison, *p*-nitrophenyl sulfate, using an implicit solvent model with increasing numbers of explicit solvent molecules included in our calculations. As expected, we see that including explicit hydrogen bonding interactions is clearly significant. That is, it affects not just the mechanistic balance between substrate- and solvent-assisted pathways by several orders of magnitude in rate, but in some cases also the transition state geometries. Despite the fact that even eight water molecules are not enough to provide completely converging energies and geometries, it is possible to obtain chemical information that is far superior to using just an implicit solvent model, at much lower computational cost than full explicit *ab initio* QM/MM or metadynamics calculations, allowing multiple pathways to be tested relatively easily.

Considering the calculated KIE for *p*NPP, the nonbridging KIE are slightly inverse for both the substrate- and solvent-assisted pathways. For the solvent-assisted pathway, this is consistent with the slight shortening of these bonds in the TS, which presumably leads to stiffer stretching and bending. For the substrate-assisted pathway the slightly more inverse KIE is presumably due to the protonation of one of the P–O in the TS, as the other two bonds show a smaller decrease in bond length in the TS. The equilibrium isotope effect for protonating a phosphate monoester is 0.985,<sup>72</sup> and so the calculated value is rather smaller than this, despite the observation that the proton transfer appears to be essentially complete by the time the TS is reached. It may be that the change in the P–O bonding is greater in reaching the phosphorane-like TS than in the RS monoesters, which compensates for the protonation. Although due to different structural effects, it appears that the nonbridging KIE is not a sensitive criterion for discriminating between the two pathways. However, the KIE at the bridging and remote <sup>15</sup>N position do provide a clear distinction and can be rationalized by the far greater change in bonding to the leaving group in the solvent-assisted pathway.

Mechanistically, it would appear that the preferred pathway is dependent on the specific leaving group. For a good aryl leaving group, the preferred mechanism is a concerted reaction with a loose transition state, and is similar for both the aryl sulfate and the aryl phosphate monoesters, consistent with previous interpretations of the experimental data (see refs 8 and 68), and in contrast to previous theoretical studies (see refs 16, 25, 55 which have argued for a more associative, substrate-assisted pathway). However, in the case of the aryl phosphates, once explicit water molecules have been introduced in the system to provide better solvation, the two mechanisms are close enough in energy that the balance between the two might easily be altered in a nonhomogenous environment such as an enzyme

active site (due to the differences in charge distribution at the two transition states), even if the discrimination is not necessarily obvious in aqueous solution. For methyl phosphate, the preferred mechanism seems to switch to an associative addition–elimination  $A_N + D_N$  process, with an intermediate that exists in a very shallow potential well. Interestingly, the differential behavior between the aryl and alkyl phosphates is in agreement with previous theoretical studies,<sup>16,73</sup> which obtained very different qualitative results for the hydrolysis of a polyphosphate and for methyl phosphate, suggesting a dissociative solvent-assisted mechanism in the former case<sup>73</sup> and an associative substrate-assisted mechanism in the latter case.<sup>16</sup> These descriptions are consistent with our calculations, which show a strong leaving group dependence, and indicates that even limited microsolvation might be sufficient to reproduce similar results to high-level calculations in full explicit solvent, but at much lower computational cost. It should be noted, however, that the almost 10 kcal/mol discrimination between TS and TS2 of Figure 6 for the hydrolysis of MP could include an overestimate due to inadequacies in the solvation of methoxide ion by the implicit solvent model (see discussion in the Supporting Information), and these two pathways are likely closer in energy than would be suggested by this figure, albeit still with a preference for the substrate-assisted pathway.

The situation is more straightforward in the case of the arylsulfate. In this case the low  $pK_a$  of this compound precludes an associative substrate-assisted mechanism and the only viable pathway is through a solvent-assisted mechanism, with a water molecule acting as a proton acceptor after bond formation to the nucleophile. Since phosphate monoesters also appear to be capable of a similar mechanism, an enzyme that has been fine-tuned to accommodate the demanding hydrolysis of sulfate monoesters could also in principle accommodate phosphate monoesters with relative ease, as is seen for example in the case of the arylsulfatase from *Pseudomonas aeruginosa* (PAS).<sup>71</sup> The opposite is not necessarily true for phosphatases,<sup>59,60,62</sup> if they have been evolutionarily optimized for the more associative pathway. We also observe that, for *p*-nitrophenyl phosphate and sulfate hydrolysis, there appears to be a structural basis to the choice of mechanism, depending on the position of the proton on the nucleophile and whether the leaving group aryl ring is coplanar with the phosphate or perpendicular to the phosphate.

The final question concerns the role of the proton transfer in the reaction, and whether it is a driving force or a simple consequence of bond formation. Recently, there has been a related debate about whether the mechanism of GTP hydrolysis by GTPases proceeds through a transition state with no deprotonation of the nucleophile, one with direct proton transfer to the phosphate,<sup>74</sup> or one with proton transfer to the phosphate through an intervening water molecule, a so-called “2-water mechanism”.<sup>74,75</sup> Our calculations on *p*NPP support a solvent assisted mechanism, a conclusion that is strengthened by the fact that this pathway reproduces the experimentally measured KIEs. Recent computational work has also suggested that the energy discrimination between a mechanism involving direct proton transfer to the phosphate and one involving an intervening water molecule is minimal,<sup>75</sup> suggesting that the pathway for protonation of the phosphate does not affect the reaction greatly.

To explore this issue further, we provide an overview of the protonation states of the nucleophile and phosphate at representative points on the calculated energy landscapes for

*p*NPP and MP hydrolysis (Figure 2A and B) in Table S15. We have also provided an overview of key P–O and O–H distances along the calculated intrinsic reaction coordinate for *p*NPP and MP hydrolysis in the presence of two explicit water molecules (from the unconstrained TS optimization) in Figure S6. From this figure and table it can be seen that, in both cases, nucleophile deprotonation and protonation of the phosphoryl group precedes attack at the phosphorus center, allowing the reaction to in effect proceed through the equivalent of a pre-equilibrium proton transfer to the phosphate. The effect of the proton transfer to the P–O will be to inhibit the expanded transition state due to the formation of a very high energy protonated metaphosphate, pushing the pathway toward the phosphorane intermediate. Likewise, if the nucleophile is not deprotonated, the trianionic phosphorane will be formed in a very high energy tautomer, and the pathway is pushed toward the expansive concerted pathway (see more extended discussion in Supporting Information).

Irrespective of whether it occurs directly or via intervening water, the protonation of the phosphoryl oxygen does however lead to the formation of a pentacoordinate intermediate in a plausible ionic state, considering the thermodynamic data gathered by Guthrie,<sup>76</sup> the calculations presented here suggest that the kinetic barriers to forming this intermediate are not large. This may differ in the reaction of a diester with hydroxide, even though this would form an intermediate with similar stability. Our calculations confirm that for both cases *p*NPP and MP, the proton transfer is coupled to changes in P–O bonding patterns and it clearly precedes bond formation to the nucleophile (Figure S10). Therefore, deprotonation of the nucleophile and generation of a hydroxide ion appears to be driving this reaction. This mechanism in turn potentially dominates for the poor alkyl leaving group, but is higher in energy in the case of the good aryl leaving group. Therefore, the nature of the leaving-group appears to have a large impact on the choice of mechanism for the hydrolyses of these phosphates, as was also seen in recent calculations.<sup>16,73</sup> This suggests it can be risky to extrapolate between experiments with highly activated aryl leaving groups<sup>23</sup> and calculations with poor alkyl leaving groups.<sup>55</sup> Overall, we present here a consistent mechanistic framework that accounts both for a key experimental observable that was not reproduced in previous theoretical studies (i.e., the kinetic isotope effects), and for apparent discrepancies between theory and experiment.

## ■ ASSOCIATED CONTENT

### Supporting Information

Energy breakdown for the different mechanisms studied in this work. Key distances, Wiberg bond indices and charges. Microscopic reversibility considerations. Comparison of substrate-assisted mechanisms involving direct proton transfer or proton transfer via an intervening water molecule. Methodological considerations: Reliability of the solvent model. Absolute energies and Cartesian coordinates of key stationary points. This material is available free of charge via the Internet at <http://pubs.acs.org>.

## ■ AUTHOR INFORMATION

### Corresponding Authors

[n.h.williams@sheffield.ac.uk](mailto:n.h.williams@sheffield.ac.uk)  
[kamerlin@icm.uu.se](mailto:kamerlin@icm.uu.se)

## Notes

The authors declare no competing financial interest.

## ■ ACKNOWLEDGMENTS

The European Research Council has provided financial support under the European Community's Seventh Framework Programme (FP7/2007-2013)/ERC Grant Agreement No. 306474. S.C.L.K. and J.Å. acknowledge support from the Swedish Research Council (VR) No. 2010-5026 and the Swedish National Infrastructure for Computing (SNIC). S.C.L.K. and N.H.W. acknowledge support from the Swedish Foundation for Internationalization in Higher Education and Research (STINT 2012-2097). The authors would like to thank Dan Singleton for assisting in the KIE calculations, and Dan Singleton, John Richard and Tony Kirby for valuable discussion.

## ■ REFERENCES

- (1) Knowles, J. R. *Annu. Rev. Biochem.* **1980**, *49*, 877.
- (2) Westheimer, F. H. *Science* **1987**, *235*, 1173.
- (3) Lad, C.; Williams, N. H.; Wolfenden, R. *Proc. Natl. Acad. Sci. U. S. A.* **2003**, *100*, 5607.
- (4) Schroeder, G. K.; Lad, C.; Wyman, P.; Williams, N. H.; Wolfenden, R. *Proc. Natl. Acad. Sci. U. S. A.* **2006**, *103*, 4052.
- (5) Zalatan, J. G.; Fenn, T. D.; Herschlag, D. *J. Mol. Biol.* **2008**, *384*, 1174.
- (6) Lassila, J. K.; Zalatan, J. G.; Herschlag, D. *Annu. Rev. Biochem.* **2011**, *80*, 669.
- (7) Kamerlin, S. C. L.; Sharma, P. K.; Prasad, R. B.; Warshel, A. *Q. Rev. Biophys.* **2013**, *46*, 1.
- (8) Hengge, A. C.; Edens, W. A.; Elsing, H. *J. Am. Chem. Soc.* **1994**, *116*, 5045.
- (9) Kirby, A. J.; Varvoglis, A. G. *J. Am. Chem. Soc.* **1967**, *89*, 415.
- (10) Kirby, A. J.; Jencks, W. P. *J. Am. Chem. Soc.* **1965**, *87*, 3209.
- (11) Yamamoto, T. *Chem. Phys. Lett.* **2010**, *500*, 263.
- (12) Klähn, M.; Rosta, E.; Warshel, A. *J. Am. Chem. Soc.* **2006**, *128*, 15310.
- (13) Florian, J.; Warshel, A. *J. Phys. Chem. B* **1998**, *102*, 719.
- (14) Kamerlin, S. C. L.; Florian, J.; Warshel, A. *ChemPhysChem* **2008**, *9*, 1767.
- (15) Iche-Tarrat, N.; Ruiz-Lopez, M.; Barthelat, J. C.; Vigroux, A. *Chem. Eur. J.* **2007**, *13*, 3617.
- (16) Li, W. J.; Rudack, T.; Gerwert, K.; Gräter, F.; Schlitter, J. *J. Chem. Theory Comput.* **2012**, *8*, 3596.
- (17) Bianciotto, M.; Barthelat, J. C.; Vigroux, A. *J. Am. Chem. Soc.* **2002**, *124*, 7573.
- (18) Åqvist, J.; Kolmodin, K.; Florian, J.; Warshel, A. *Chem. Biol.* **1999**, *6*, R71.
- (19) Kamerlin, S. C. L.; Wilkie, J. *Org. Biomol. Chem.* **2011**, *9*, 5394.
- (20) Rosta, E.; Kamerlin, S. C. L.; Warshel, A. *Biochemistry* **2008**, *47*, 3725.
- (21) Schweins, T.; Langen, R.; Warshel, A. *Nat. Struct. Biol.* **1994**, *1*, 476.
- (22) Adamczyk, A. J.; Warshel, A. *Proc. Natl. Acad. Sci. U. S. A.* **2011**, *108*, 9827.
- (23) Admiraal, S. J.; Herschlag, D. *J. Am. Chem. Soc.* **2000**, *122*, 2145.
- (24) We note that mechanisms A and C violate microscopic reversibility if the leaving group is identical to the nucleophile, and applying microscopic reversibility is appropriate where the leaving group is very similar to the incoming nucleophile (e.g., when water displaces methanol). To avoid this, it is necessary that there are additional mechanisms that involve initial proton transfer, followed by attack of hydroxide on the protonated species. The reverse of the mechanism shown: Burwell, R. L.; Pearson, R. G. *J. Phys. Chem.* **1966**, *70*, 300. These pathways would provide free energy profiles that are the reflection of the ones shown and would involve rate limiting transition states that are very similar to each other (e.g., exchange of

methyl and a proton in the case of MP hydrolysis). These additional pathways are illustrated explicitly in the Supporting Information.

- (25) Kamerlin, S. C. L. *J. Org. Chem.* **2011**, *76*, 9228.
- (26) Zhang, L. D.; Xie, D. Q.; Xu, D. G.; Guo, H. *Chem. Commun.* **2007**, 1638.
- (27) Ferreira, D. E. C.; Florentino, B. P. D.; Rocha, W. R.; Nome, F. *J. Phys. Chem. B* **2009**, *113*, 14831.
- (28) Hoff, R. H.; Larsen, P.; Hengge, A. C. *J. Am. Chem. Soc.* **2001**, *123*, 9338.
- (29) Benkovic, S. J.; Benkovic, P. A. *J. Am. Chem. Soc.* **1966**, *88*, 5504.
- (30) O'Ferrall, R. A. *J. Chem. Soc. B* **1970**, 274.
- (31) Jencks, W. P. *Chem. Rev.* **1985**, *85*, 511.
- (32) Zhao, Y.; Truhlar, D. G. *Theor. Chem. Acc.* **2008**, *120*, 215.
- (33) Marenich, A. V.; Cramer, C. J.; Truhlar, D. G. *J. Phys. Chem. B* **2009**, *113*, 6378.
- (34) Xia, F. T.; Zhu, H. *J. Comput. Chem.* **2011**, *32*, 2545.
- (35) Kamerlin, S. C. L.; Haranczyk, M.; Warshel, A. *ChemPhysChem* **2009**, *10*, 1125.
- (36) Kelly, C. P.; Cramer, C. J.; Truhlar, D. G. *J. Phys. Chem. A* **2006**, *110*, 2493.
- (37) The substitution of H with  $\text{PO}_3^{2-}$  in  $\text{H}_2\text{O}$  leads to a 3.4 unit depression in  $\text{p}K_a$  (15.7 for  $\text{HO}-\text{H}$  compared to 12.3 for  $\text{HO}-\text{PO}_3^{2-}$ ). Applying this change to the  $\text{p}K_a$  of  $\text{H}_3\text{O}^+$  would lead to an estimate around  $-1.7 - 3.4 = -5$  for the initial product. Kirby, A. J.; Varvoglis, A. G. *J. Am. Chem. Soc.* **1967**, *89*, 405 provides estimates of related species as similarly acidic (about  $-4$ ), which accounts for the observed reactivity of methyl phosphate monoanions convincingly, and suggests that this species is transiently viable. Considering cations, the substitution of H with  $\text{PO}_3^{2-}$  in  $\text{NH}_4^+$  leads to a rather smaller depression in  $\text{p}K_a$  ( $\text{H}_3\text{N}^+-\text{PO}_3^{2-} \sim 1$  unit more acidic than  $\text{H}_3\text{N}^+-\text{H}$ ).
- (38) Hratchian, H. P.; Schlegel, H. B. *J. Chem. Phys.* **2004**, *120*, 9918.
- (39) Hratchian, H. P.; Schlegel, H. B. *J. Chem. Theory Comput.* **2005**, *1*, 61.
- (40) Alecu, I. M.; Zheng, J. J.; Zhao, Y.; Truhlar, D. G. *J. Chem. Theory Comput.* **2010**, *6*, 2872.
- (41) Alexeev, Y.; Windus, T. L.; Zhan, C. G.; Dixon, D. A. *Int. J. Quantum Chem.* **2005**, *102*, 775.
- (42) Ribeiro, A. J. M.; Ramos, M. J.; Fernandes, P. A. *J. Chem. Theory Comput.* **2010**, *6*, 2281.
- (43) Frisch, M. J.; Trucks, G. W.; Schlegel, H. B.; Scuseria, G. E.; Robb, M. A.; Cheeseman, J. R.; Scalmani, G.; Barone, V.; Mennucci, B.; Petersson, G. A.; Nakatsuji, H.; Caricato, M.; Li, X.; Hratchian, H. P.; Izmaylov, A. F.; Bloino, J.; Zheng, G.; Sonnenberg, J. L.; Hada, M.; Ehara, M.; Toyota, K.; Fukuda, R.; Hasegawa, J.; Ishida, M.; Nakajima, T.; Honda, Y.; Kitao, O.; Nakai, H.; Vreven, T.; Montgomery, J. A., Jr.; Peralta, J. E.; Ogliaro, F.; Bearpark, M.; Heyd, J. J.; Brothers, E.; Kudin, K. N.; Staroverov, V. N.; Kobayashi, R.; Normand, J.; Raghavachari, K.; Rendell, A.; Burant, J. C.; Iyengar, S. S.; Tomasi, J.; Cossi, M.; Rega, N.; Millam, J. M.; Klene, M.; Knox, J. E.; Cross, J. B.; Bakken, V.; Adamo, C.; Jaramillo, J.; Gomperts, R.; Stratmann, R. E.; Yazyev, O.; Austin, A. J.; Cammi, R.; Pomelli, C.; Ochterski, J. W.; Martin, R. L.; Morokuma, K.; Zakrzewski, V. G.; Voth, G. A.; Salvador, P.; Dannenberg, J. J.; Dapprich, S.; Daniels, A. D.; Farkas, Ö.; Foresman, J. B.; Ortiz, J. V.; Cioslowski, J.; Fox, D. J. *Gaussian 09*, Revision C01; Gaussian, Inc.: Wallingford, CT, 2009.
- (44) Bigeleisen, J.; Mayer, M. G. *J. Chem. Phys.* **1947**, *15*, 261.
- (45) Wolfsberg, M. *Acc. Chem. Res.* **1972**, *5*, 225.
- (46) Saunders, M.; Laidig, K. E.; Wolfsberg, M. *J. Am. Chem. Soc.* **1989**, *111*, 8989.
- (47) Duarte, F.; Gronert, S.; Kamerlin, S. C. L. *J. Org. Chem.* **2014**, *79*, 1280.
- (48) Guthrie, J. P. *J. Am. Chem. Soc.* **1996**, *118*, 12878.
- (49) Allen, F. H. *Acta Crystallogr., Sect. B: Struct. Sci.* **2002**, *58*, 380.
- (50) López-Canut, V.; Ruiz-Pernía, J.; Tuñón, I.; Ferrer, S.; Moliner, V. *J. Chem. Theory Comput.* **2009**, *5*, 439.
- (51) Cleland, W. W.; Hengge, A. C. *Chem. Rev.* **2006**, *106*, 3252.
- (52) Wang, Y. N.; Topol, I. A.; Collins, J. R.; Burt, S. K. *J. Am. Chem. Soc.* **2003**, *125*, 13265.
- (53) Branduardi, D.; De Vivo, M.; Rega, N.; Barone, V.; Cavalli, A. *J. Chem. Theory Comput.* **2011**, *7*, 539.
- (54) Yang, Y.; Yu, H. B.; York, D.; Elstner, M.; Cui, Q. *J. Chem. Theory Comput.* **2008**, *4*, 2067.
- (55) Florían, J.; Warshel, A. *J. Am. Chem. Soc.* **1997**, *119*, 5473.
- (56) Kamerlin, S. C.; Williams, N. H.; Warshel, A. *J. Org. Chem.* **2008**, *73*, 6960.
- (57) Duarte, F.; Geng, T.; Marloie, G.; Al Hussain, A. O.; Williams, N. H.; Kamerlin, S. C. L. *J. Org. Chem.* **2014**, *79*, 2816.
- (58) Khersonsky, O.; Tawfik, D. S. *Annu. Rev. Biochem.* **2010**, *79*, 471.
- (59) Jonas, S.; Hollfelder, F. *Pure Appl. Chem.* **2009**, *81*, 731.
- (60) Mohamed, M. F.; Hollfelder, F. *Biochim. Biophys. Acta* **2013**, *1834*, 417.
- (61) Duarte, F.; Amrein, B. A.; Kamerlin, S. C. L. *Phys. Chem. Chem. Phys.* **2013**, *15*, 11160.
- (62) Babbie, A.; Tokuriki, N.; Hollfelder, F. *Curr. Opin. Chem. Biol.* **2010**, *14*, 200.
- (63) Edwards, D. R.; Lohman, D. C.; Wolfenden, R. *J. Am. Chem. Soc.* **2012**, *134*, 525.
- (64) Williams, S. J.; Denehy, E.; Krenske, E. H. *J. Org. Chem.* **2014**, *79*, 1995.
- (65) Bourne, N.; Williams, A. *J. Org. Chem.* **1984**, *49*, 1200.
- (66) Gibby, S. G.; Younker, J. M.; Hengge, A. C. *J. Phys. Org. Chem.* **2004**, *17*, 541.
- (67) Kolthoff, I. M. *Treatise on Analytical Chemistry*; Interscience Encyclopedia, Inc.: New York, 1959.
- (68) Hengge, A. C. *Acc. Chem. Res.* **2002**, *35*, 105.
- (69) O'Brien, P. J.; Herschlag, D. *J. Am. Chem. Soc.* **1998**, *120*, 12369.
- (70) Catrina, I.; O'Brien, P. J.; Purcell, J.; Nikolic-Hughes, I.; Zalatan, J. G.; Hengge, A. C.; Herschlag, D. *J. Am. Chem. Soc.* **2007**, *129*, 5760.
- (71) Olguin, L. F.; Askew, S. E.; O'Donoghue, A. C.; Hollfelder, F. *J. Am. Chem. Soc.* **2008**, *130*, 16547.
- (72) Knight, W. B.; Weiss, P. M.; Cleland, W. W. *J. Am. Chem. Soc.* **1986**, *108*, 2759.
- (73) Graves, R.; Mathias, G.; Marx, D. *J. Am. Chem. Soc.* **2012**, *134*, 6995.
- (74) Prasad, B. R.; Plotnikov, N. V.; Lameira, J.; Warshel, A. *Proc. Natl. Acad. Sci. U. S. A.* **2013**, *110*, 20509.
- (75) Plotnikoy, N. V.; Prasad, B. R.; Chakrabarty, S.; Chu, Z. T.; Warshel, A. *J. Phys. Chem. B* **2013**, *117*, 12807.
- (76) Guthrie, J. P. *J. Am. Chem. Soc.* **1977**, *99*, 3991.